LEGIBILITY NOTICE

A major purpose of the Technical Information Center is to provide the broadest dissemination possible of information contained in DOE's Research and Development Reports to business, industry, the academic community, and federal, state and local governments.

Although a small portion of this report is not reproducible, it is being made available to expedite the availability of information on the research discussed herein.

PR#0596-7

ornl

ORNL/TM-10947

OAK RIDGE
NATIONAL
LABORATORY

MARTIN MARIETTA

Nonlinear Dynamics of Single-Helicity Neoclassical MHD Tearing Instabilities

D. A. Spong
K. C. Shaing
B. A. Carreras
J. D. Callen
L. Garcia

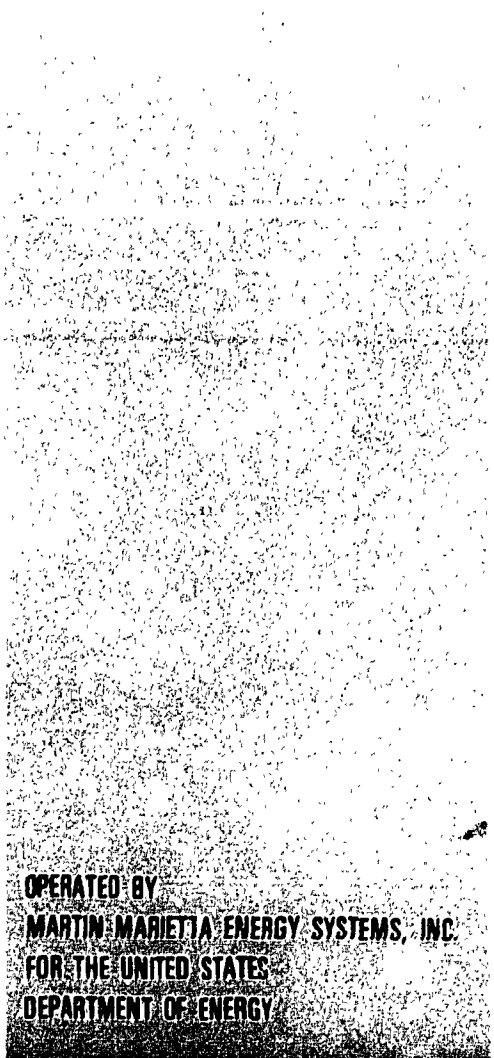

OPERATED BY
MARTIN MARIETTA ENERGY SYSTEMS, INC.
FOR THE UNITED STATES
DEPARTMENT OF ENERGY

Printed in the United States of America. Available from
National Technical Information Service
U.S. Department of Commerce
5285 Port Royal Road, Springfield, Virginia 22161
NTIS price codes—Printed Copy: A03; Microfiche A01

ORNL/TM-10947
Dist. Category UC-427

ORNL/TM--10947

DE89 001960

Fusion Energy Division

NONLINEAR DYNAMICS OF SINGLE-HELICITY NEOCLASSICAL MHD TEARING INSTABILITIES

D. A. Spong
K. C. Shaing
B. A. Carreras

J. D. Callen
University of Wisconsin, Madison, Wisconsin 53706

L. Garcia
Universidad Complutense, Madrid, Spain

Date published: October 1988

Prepared by the
OAK RIDGE NATIONAL LABORATORY
Oak Ridge, Tennessee 37831
operated by
MARTIN MARIETTA ENERGY SYSTEMS, INC.
for the
U.S. DEPARTMENT OF ENERGY
under contract DE-AC05-84OR21400

CONTENTS

ABSTRACT v
I. INTRODUCTION 1
II. TIME-EVOLUTION EQUATIONS 3
III. NUMERICAL RESULTS 6
IV. CONCLUSIONS 11
REFERENCES 13

ABSTRACT

Neoclassical magnetohydrodynamic (MHD) effects can significantly alter the nonlinear evolution of resistive tearing instabilities. This is studied numerically by using a flux-surface-averaged set of evolution equations that includes the lowest-order neoclassical MHD effects. The new terms in the equations are fluctuating bootstrap current, neoclassical modification of the resistivity, and neoclassical damping of the vorticity. Single-helicity tearing modes are studied in a cylindrical model over a range of neoclassical viscosities (μ_e/ν_e) and values of the Δ' parameter of tearing mode theory. Increasing the neoclassical viscosity leads to increased growth rate and saturated island width as predicted analytically. The larger island width is caused by the fluctuating bootstrap current contribution in Ohm's law. The Δ' parameter no longer solely determines the island width, and finite-width saturated islands may be obtained even when Δ' is negative. The importance of the bootstrap current ($\sim\partial\rho/\partial\psi$) in the nonlinear dynamics leads us to examine the sensitivity of the results with respect to different models for the density evolution.

I. INTRODUCTION

The single-helicity nonlinear behavior of resistive tearing instabilities[1,2] has been an important ingredient in understanding the disruption physics and plasma confinement properties of tokamaks.[3,4] It is therefore of significant interest to extend the analysis of such instabilities from the low-temperature, resistive regime into the high-temperature, long-mean-free-path regime characteristic of most present experiments. This has recently become possible with the development[5–7]of a set of neoclassical magnetohydrodynamic (MHD) equations, which extend the widely used resistive MHD model from the Pfirsch-Schlüter collisionality regime to the experimentally relevant banana-plateau regime. These equations include a number of new phenomena that are unique to the long-mean-free-path regime, such as the fluctuating bootstrap current contribution to Ohm's law, the enhanced (by B^2/B_θ^2) polarization drift and perpendicular dielectric constant, and the rapid viscous damping of the poloidal ion flow velocity. In this report, we discuss the first numerical calculations of tearing instabilities using these equations.

Nonlinear tearing mode evolution for the small-island-width regime has recently been calculated analytically by using simplified neoclassical MHD equations.[8,9] These are generally based on cylindrical flux-surface-averaged tokamak models with the primary neoclassical MHD effect being the fluctuating bootstrap current in Ohm's law. They are limited to island widths that are large relative to the singular layer width (so that inertial effects contained in the vorticity equation are unimportant) but small relative to the resonant surface radius. An enhancement in the island width is found along with a new nonlinear growth regime where the island width increases at a $t^{1/2}$ rate. This regime exists between the exponential and Rutherford[1] linear growth stages.

The model used in this paper is also based on a flux-surface-averaged set of neoclassical MHD equations,[5,6] which are solved in a cylindrical tokamak geometry. In addition to the fluctuating bootstrap current, the neoclassical modification to the resistivity and viscous damping in the vorticity equation are included; however, we find that the latter two terms are not generally as important as the bootstrap current. These equations are evolved in time by using the mostly explicit version of the KITE initial value code.[10] Both the exponential, neoclassical ($\sim t^{1/2}$), Rutherford and fully nonlinear regimes can be examined. In addition to the flux and vorticity equations, the numerical calculation includes a density evolution equation. This

equation does not include any neoclassical MHD effects directly, but it has an important influence on the neoclassical tearing mode evolution through the bootstrap current term in Ohm's law. In this paper, we consider two models of the density evolution: convection alone and and convection with parallel diffusion along field lines. Also, in both models a small level of perpendicular density diffusion is present for numerical stability purposes.

The basic parameter that determines the strength of the neoclassical MHD terms in our equations will be the ratio of electron viscosity to collision frequency (μ_e/ν_e). In the low-frequency banana regime, $\mu_e/\nu_e \simeq 2.3\sqrt{\epsilon} \simeq 1$; in the plateau regime, $\mu_e/\nu_e \simeq \sqrt{\epsilon}/\nu_{*e}$ ($\nu_{*e} = \nu_e \epsilon^{-3/2} R_0 q/v_{th,e}$). In the collisional Pfirsch-Schlüter regime, $\mu_e/\nu_e \to 0$. Thus, we typically vary μ_e/ν_e over the range from 0 to 1. At moderate values of the neoclassical electron viscosity parameter ($0 < \mu_e/\nu_e \lesssim 0.4$), both density evolution models indicate an increase in the saturated island width with increasing μ_e/ν_e. At higher values ($0.5 \lesssim \mu_e/\nu_e \leq 1$), the island width behavior becomes more sensitive to the density model. For the case with convection only, the width may fail to attain a saturated value or become practically independent of μ_e/ν_e. When parallel diffusion is present, the island width continues to increase at the higher values of μ_e/ν_e but eventually levels off near $\mu_e/\nu_e \simeq 1$. Both models tend to give saturated island widths that are smaller than the analytic calculations at large values of μ_e/ν_e but that are still significantly larger than the $\mu_e/\nu_e = 0$ case. This difference was expected because of the assumptions of small island width in the analysis.

In addition to the dependence on μ_e/ν_e, a second feature of neoclassical tearing modes, which is of interest, is the dependence on Δ'. For linear tearing mode stability, the energy δW is directly proportional to Δ' [defined following Eq. (16)]. With neoclassical MHD, linear instability and finite saturated islands are possible with Δ' both positive and negative. We consider a range of Δ' values here by varying $q(0)$ (central q value) and find that unstable tearing mode growth and saturation can easily be obtained for $\Delta' < 0$ cases that would otherwise be stable without neoclassical MHD.

The outline of this paper is as follows. Section II presents the analysis and basic equations used in the numerical calculations and describes the density evolution models. In Sec. III, the numerical results for the various models are presented and compared with the analytical results. A conclusion and summary are given in Sec. IV.

II. TIME-EVOLUTION EQUATIONS

The basic equations underlying the calculations of this paper are the neoclassical moment equations[5,6] for the electron density n_e, poloidal flux ψ, velocity stream function ϕ, and parallel ion velocity $V_{\|i}$. These equations, given below in mks units, result from using the electron continuity equation, Ohm's law, and the perpendicular and parallel ion momentum equations:

$$\frac{\partial n_e}{\partial t} = -\vec{\nabla}\cdot(n_e\vec{v}_{\perp e}) - (\vec{B}\cdot\vec{\nabla})\left[\frac{n_e}{B}\left(V_{\|i} - \frac{J_\|}{en_e}\right)\right] \quad , \tag{1}$$

$$-\frac{F}{R^2}\frac{\partial\psi}{\partial t} = -\frac{J_\| B}{\sigma_\|} - (\vec{B}\cdot\vec{\nabla})\left(\phi - \frac{T_e}{e}\ln n_e\right) + \frac{1}{en_e}\vec{B}\cdot(\vec{\nabla}\cdot\overleftrightarrow{\Pi}_{\|e}) \quad , \tag{2}$$

$$\vec{\nabla}\cdot\left[\frac{\rho_m}{B^2}\vec{B}\times\left(\frac{\partial}{\partial t} + \vec{v}_E\cdot\vec{\nabla}\right)\vec{v}_{\perp i}\right] = -(\vec{B}\cdot\vec{\nabla})\left(\frac{J_\|}{B}\right) - \vec{\nabla}\cdot\left(\frac{1}{B^2}\vec{B}\times\vec{\nabla}p\right) - \vec{\nabla}\cdot\left(\frac{\vec{B}\times\vec{\nabla}\cdot\overleftrightarrow{\Pi}_{\|i}}{B^2}\right) \quad , \tag{3}$$

$$\rho_m\left(\frac{\partial}{\partial t} + \vec{v}_E\cdot\vec{\nabla}\right)(V_{\|i}B) = -(\vec{B}\cdot\vec{\nabla})p - \vec{B}\cdot(\vec{\nabla}\cdot\overleftrightarrow{\Pi}_{\|i}) \quad , \tag{4}$$

where

$$\vec{v}_E = \frac{\vec{B}}{B^2}\times\vec{\nabla}\phi \quad ,$$

$$J_\| = \frac{B}{\mu_0 F}R^2\vec{\nabla}\cdot(R^{-2}\vec{\nabla}\psi)[1+\mathcal{O}(\epsilon^2)] = n_e e(V_{\|i} - V_{\|e}) \quad ,$$

$$\vec{v}_{\perp s} = \frac{\vec{B}}{B^2}\times\vec{\nabla}\left(\phi + \frac{T_s}{q_s}\ln n\right) \quad ,$$

$$\vec{B} = F\vec{\nabla}\zeta + \vec{\nabla}\psi\times\vec{\nabla}\zeta \quad ,$$

$\rho_m = n_i m_i$ is the ion mass density.

The viscous stress terms in Eqs. (1)–(4) may be related to the neoclassically driven pressure anisotropy. This is given by ($\hat{b} \equiv \vec{B}/B$)

$$\overleftrightarrow{\Pi}_\| = (p_\| - p_\perp)(\hat{b}\hat{b} - \overleftrightarrow{I}/3) \tag{5}$$

where $p_\| - p_\perp$ for species s may be expressed in terms of the viscous damping frequency μ_s, the magnetic field B, mass density $n_s m_s$, and flow velocity $\vec{V}_s$ as follows:

$$(p_\| - p_\perp)_s = -\frac{m_s n_s \mu_s \langle B^2\rangle}{\langle(\hat{b}\cdot\vec{\nabla}B)^2\rangle}(\vec{V}_s\cdot\vec{\nabla}\ln B) \tag{6}$$

with

$$\vec{V}_s \cdot \vec{\nabla} \ln B = U_{\theta s}(\hat{b} \cdot \vec{\nabla} B) + V_{rs} \frac{\partial \ln B}{\partial r}$$

and

$$U_{\theta s} = \frac{\vec{V}_s \cdot \vec{\nabla}\theta}{\vec{B} \cdot \vec{\nabla}\theta} = \frac{V_{\|s}}{B} + \frac{F}{B^2} \frac{\partial}{\partial \psi} \left(\phi + \frac{T_s}{q_s} \ln n_s \right) \quad .$$

Equations (1)–(4) are inherently three-dimensional (3-D) and contain significant toroidal couplings through the neoclassical MHD terms (i.e., from the $\hat{b} \cdot \vec{\nabla} B$ and $\partial \ln B / \partial r$ coefficients in the viscous stress terms). These couplings are of importance for unfavorable curvature–pressure-gradient-driven instabilities, as discussed elsewhere.[11] However, for current-gradient-driven tearing instabilities, it is reasonable as a first step to reduce these equations to a cylindrical geometry to avoid the complexity of fully toroidal, nonlinear calculations. This can be accomplished by performing a flux surface average of each evolution equation. The averaged neoclassical parallel and cross viscous stress terms then become in cylindrical geometry:

$$\left\langle \vec{B} \cdot \vec{\nabla} \cdot \overleftrightarrow{\Pi}_{\|} \right\rangle_s = m_s n_s \mu_s \left\langle B^2 \right\rangle U_{\theta s} \tag{7}$$

and

$$\left\langle \vec{\nabla} \cdot \left(\frac{1}{B^2} \vec{B} \times \vec{\nabla} \cdot \overleftrightarrow{\Pi}_{\|} \right) \right\rangle_s \simeq \frac{1}{r} \frac{\partial}{\partial r} (r \alpha_s V_{\theta s}) - \frac{1}{r} \frac{\partial}{\partial \theta} (\alpha_s V_{rs}) \quad , \tag{8}$$

where

$$\alpha_s = \frac{m_s n_s \mu_s \langle B^2 \rangle}{2 B_0 \langle (\hat{b} \cdot \vec{\nabla} B)^2 \rangle R_0^2} \quad ,$$

R_0 and B_0 are the major radius and magnetic field at $r = 0$, and the angle brackets $\langle \ldots \rangle$ indicate a flux surface average. Here, an (r, θ, ζ) cylindrical coordinate system is used, where r $(0 < r < a)$ is the radial coordinate, a is the radius of the cylinder, θ is the poloidal angle, and ζ is an angle-like coordinate such that $\zeta = 2\pi z / L$, where z is the coordinate along the axis of the cylinder of length $L = 2\pi R_0$.

We further simplify Eqs. (1)–(4) by assuming rapid damping of the ion poloidal flow relative to the tearing instability time scale (i.e., $\langle \vec{B} \cdot \vec{\nabla} \cdot \overleftrightarrow{\Pi}_{\|i} \rangle \simeq 0$). This results in the following equations for $V_{\|i}$ and $V_{\|e}$ in terms of the potential ϕ and parallel current $J_{\|}$:

$$V_{\|i} = -R_0 \frac{\partial \phi}{\partial \psi} \quad , \tag{9}$$

$$V_{\|e} = -R_0 \frac{\partial \phi}{\partial \psi} - \frac{J_{\|}}{en} \quad . \tag{10}$$

The $V_{\|i}$ evolution equation (4) then does not need to be retained and can be replaced by Eq. (9). Also, we take $T_i = 0$ (except that μ_i is kept finite), $T_e =$ constant, and

approximate $F \simeq R_0 B_0$, $\langle B^2 \rangle \simeq B_0^2$, $R \simeq R_0$, and $J_\parallel \simeq J_\zeta$, as is appropriate to cylindrical geometry. The three equations for $\tilde{\psi}, \tilde{U}$ $[= \vec{\nabla}_\perp \cdot (\rho_{eq} \vec{\nabla}_\perp \tilde{\phi})]$, and $\tilde{\rho}_m$ (mass density) are then given in nondimensional form as

$$\frac{\partial \tilde{\psi}}{\partial t} = -\nabla_\parallel \tilde{\phi} + S^{-1} \left(\eta_{eq} + \frac{\mu_e/\nu_e}{\alpha_e \rho_{eq}} \right) \tilde{J}_\zeta + \frac{(\mu_e/\nu_e)\beta_0}{2\epsilon^2 S \rho_{eq} \alpha_e} \left(\widetilde{\frac{\partial \rho_m}{\partial \psi}} \right) \quad , \tag{11}$$

$$\frac{\partial \tilde{U}}{\partial t} = [\tilde{U}, \tilde{\phi}] - \nabla_\parallel \tilde{J}_\zeta + \frac{(\mu_i \tau_{Hp}) \rho_{eq} q^2}{\epsilon^2 r^2} \frac{\partial^2 \tilde{\phi}}{\partial \theta^2} + R_U^{-1} \nabla_\perp^2 \tilde{U} \quad , \tag{12}$$

$$\frac{\partial \tilde{\rho}_m}{\partial t} = -\frac{1}{r} \frac{d\rho_{eq}}{dr} \frac{\partial \tilde{\phi}}{\partial \theta} + [\tilde{\rho}_m, \tilde{\phi}] + R_\rho^{-1} \nabla_\perp^2 \tilde{\rho}_m + \chi_{\parallel \rho} \nabla_\parallel^2 \tilde{\rho}_m \quad , \tag{13}$$

where α_e is the Spitzer resistivity coefficient (taken as 0.506 here), $S = \tau_R/\tau_{Hp}$, β_0 is the plasma beta at $r = 0$, $\tau_R = \mu_0 a^2/\eta_0$, $\tau_{Hp} = R_0/v_A$,

$$[a, b] = \frac{1}{r} \frac{\partial a}{\partial \theta} \frac{\partial b}{\partial r} - \frac{1}{r} \frac{\partial a}{\partial r} \frac{\partial b}{\partial \theta}, \quad \nabla_\parallel \tilde{f} = \hat{b} \cdot \vec{\nabla} \tilde{f} = \left(\frac{\partial}{\partial \zeta} - \frac{1}{q} \frac{\partial}{\partial \theta} \right) \tilde{f} - [\tilde{\psi}, \tilde{f}] \quad ,$$

and variables with subscript "eq" are equilibrium while those with a tilde " ~ " over them are perturbations from the equilibrium. If neither is present, then the variable is the sum of the equilibrium and perturbed components.

Perpendicular diffusion terms are present in each of the three equations, as is appropriate to classical dissipative processes. In the density equation, the coefficient of the perpendicular diffusion term will generally be larger than its classical value for the purpose of numerical stability (i.e., if this equation becomes purely convective, then grid separation problems arise). However, the coefficient R_ρ^{-1} is kept at a level of diffusion that is still much slower than the instability time scale and should not significantly modify the time-evolution characteristics. The parallel diffusion term ($\chi_{\parallel \rho}$) in the density evolution equation is a phenomenological loss term used to simulate rapid losses along field lines within a magnetic island. The coefficients R_U^{-1}, R_ρ^{-1}, and $\chi_{\parallel \rho}$ are normalized to a^2/τ_{Hp}, where a is the minor plasma radius. All times are normalized to τ_{Hp}, $\nabla_\parallel$ is normalized by R_0, $\nabla_\perp$ is normalized by a, r is normalized to a, the resistivity to η_0 (its value at $r = 0$), J_ζ to $B_{\zeta 0}/\mu_0 R_0$, ϕ to $a^2 B_0/\tau_{Hp}$, ψ to $a^2 B_0$, and the vorticity U to $\rho_m(r = 0) B_0/\tau_{Hp}$.

The neoclassical electron viscosity coefficient is normalized to the electron collision frequency (μ_e/ν_e) and typically ranges from 0 (Pfirsch-Schlüter regime) to $2.3\sqrt{\epsilon}$ (banana regime). The neoclassical ion viscosity (normalized to τ_{Hp}) may be expressed approximately in terms of μ_e/ν_e as

$$\mu_i \tau_{Hp} \simeq 0.287 \left(\frac{\mu_e}{\nu_e}\right) \sqrt{\frac{m_i}{m_e}} \frac{\epsilon^2 \omega_{cyi}^2}{\alpha_e S} \quad ,$$

where $\omega_{cyi} = \omega_{ci}\tau_{Hp}$.

The initial condition for the code is based on an exact velocity-free equilibrium solution of Eqs. (11)–(13). For such a state, $\phi = U = 0$, and $J_{\zeta,eq}$ and ψ_{eq} are obtained from an assumed equilibrium q profile, which is modeled as

$$q(r) = q_0 \left[1 + \left(\frac{r}{r_0}\right)^{2\lambda}\right]^{1/\lambda} \quad , \tag{14}$$

with q_0, λ, and r_0 as variable parameters. The relations $\partial\psi_{eq}/\partial r = -r/q(r)$ and $J_{\zeta,eq} = \nabla_\perp^2 \psi_{eq}$ are then used for $J_{\zeta,eq}(r)$ and $\psi_{eq}(r)$. The equilibrium density profile is

$$\rho_{eq}(r) = (1-\rho_0)(1-r^2)^2 + \rho_0 \quad ,$$

with ρ_0 as the edge density.

The fluctuating bootstrap current [final term in Eq. (11)] is expressed by using a Taylor expansion as follows:

$$\widetilde{\frac{\partial \rho_m}{\partial \psi}} \simeq \left(\frac{\partial \psi_{eq}}{\partial r}\right)^{-1} \left[\frac{\partial \tilde{\rho}_m}{\partial r} - \left(\frac{\partial \psi_{eq}}{\partial r}\right)^{-1} \left(\frac{\partial \rho_{eq}}{\partial r}\frac{\partial \tilde{\psi}}{\partial r} + \frac{\partial \tilde{\psi}}{\partial r}\frac{\partial \tilde{\rho}_m}{\partial r}\right)\right] \quad . \tag{15}$$

Here the equilibrium component has been subtracted out. The validity of this expansion has been checked, indicating that the last two terms cause only minor modifications to the island evolution.

III. NUMERICAL RESULTS

Equations (11)–(13) are solved in a cylindrical (r, θ, ζ) coordinate system by using Fourier expansions in θ and ζ with mode numbers m and n, respectively. The radial coordinate r is treated by using a finite difference grid. The equations are then evolved in time by using the mostly explicit algorithm in the KITE code.[10] Parameters that remain fixed for these calculations are the magnetic Reynolds number, $S = 10^5$; the density and vorticity diffusion coefficients, $R_\rho^{-1} = 2 \times 10^{-6}$ and $R_U^{-1} = 10^{-5}$; the ion cyclotron frequency parameter, $\omega_{cyi} = \omega_{ci}\tau_{Hp} = 30$; the inverse aspect ratio, $\epsilon = 0.25$; the central plasma, $\beta_0 = 0.02$; the edge density, $\rho_0 = 0.5$; the q profile parameter, $r_0 = 0.56$; and the helicity, $m/n = 2$. We typically use a set of 8 modes [$(m/n) = (0/0)$, $(2/1)$, $(4/2)$, $(6/3)$, $(8/4)$, $(10/5)$, $(12/6)$, and

(14/7)] in the numerical calculations with 200 radial grid points. A profile factor $[1-\exp(-r^2/r_b^2)]$ is introduced into the neoclassical viscosities to give the expected r^2 behavior near $r=0$ and a constant value away from the central region. We have taken $r_b = 0.25$ here.

Before presenting the numerical results, we briefly review the analytic theory[8,9] of neoclassical tearing modes. The predicted island evolution at times between the exponential growth phase and saturated nonlinear regimes is described by

$$\frac{dW}{dt} = \frac{1.66}{S}\frac{\eta(r_s)}{\eta(0)}\left[\Delta'_{mn}(W) - m^2\frac{W}{r_s^2} + \frac{C_b L_q \beta_p}{W L_p}\left(\frac{\mu_e}{\nu_e}\right)\right] \quad , \tag{16}$$

where $C_b \simeq 4.7$, W is the island width,

$$\Delta'_{mn} \equiv \lim_{\delta\to 0}\left(\left.\frac{d\psi_{mn}}{dr}\right|_{r_+} - \left.\frac{d\psi_{mn}}{dr}\right|_{r_-}\right)[\psi_{mn}(r_s)]^{-1} \ ,$$

$$q(r_s) = m/n,$$

$$L_q^{-1} = \left.\frac{1}{q}\frac{dq}{dr}\right|_{r_s},$$

$$L_p^{-1} = \left|\frac{1}{p}\frac{dp}{dr}\right|_{r_s} ,$$

$$\beta_p = \left.\frac{2\mu_0 p}{B_p^2}\right|_{r_s} ,$$

r_s = radius of resonant $q = m/n$ surface, and $r_\pm = r_s \pm \delta$.
The island width and radial positions r and r_s have been normalized to a, the minor radius. The time is normalized to τ_{Hp}, the Alfvén time. The first two terms in the brackets are the conventional resistive tearing mode island growth terms.[1,2] The third term is the contribution of fluctuating bootstrap current to island growth. Equation (16) is applicable for island widths in the range $r_s n^{-1/3} S^{-1/3} < W \ll r_s$. The function $\Delta'_{m,n}(W) - m^2 W/r_s^2$ can typically be approximated as $\simeq \Delta'_0(1 - W/W_{sat})$ with W_{sat} being the saturated island width without neoclassical MHD effects and Δ'_0 being the discontinuity in the radial derivative of the flux function at the singular surface with infinitesimal island width. For example, if we choose $r_0 = 0.56$, $q(0) = 1.34$, and $m/n = 2$, then for $\lambda = 1$ and $\Delta'_0 \simeq 10.7$, $W_{sat} \simeq 0.116$; for $\lambda = 2$ and $\Delta'_0 \simeq 13.8$, $W_{sat} \simeq 0.264$.

The neoclassical MHD saturated island width is obtained by setting $dW/dt = 0$ in Eq. (16) and solving for W:

$$W(t\to\infty) = \frac{W_{sat}}{2}\left\{1 + \left[1 + \frac{4}{W_{sat}}\frac{C_b}{\Delta'_0}\frac{L_q}{L_p}\beta_p\left(\frac{\mu_e}{\nu_e}\right)\right]^{1/2}\right\} \ . \tag{17}$$

The preceding limit indicates that the island width should increase monotonically with increasing μ_e/ν_e. The time evolution prior to reaching saturation is also of interest. If $\mu_e/\nu_e \ll 1$, then

$$W(t) = W_{sat} + \exp[-1.66\eta(r_s)\Delta_0' t/\eta(0)SW_{sat}]\,[-W_{sat} + W(0)] \qquad (18)$$

$$\simeq \begin{cases} W(0) + \dfrac{1.66}{S}\dfrac{\eta(r_s)}{\eta(0)}\Delta_0' t, & \text{for } W(t) \ll W_{sat}; \\ W_{sat}, & \text{for } t \to \infty\ , \end{cases} \qquad (19)$$

where $W(0)$ is the initial ($t = 0$) island width.

For cases where the neoclassical term dominates, a different scaling with time results[8,9]:

$$W(t) \simeq \left[W^2(0) + 3.32\frac{\eta(r_s)}{\eta(0)}\frac{C_b L_q \beta_p}{SL_p}\left(\frac{\mu_e}{\nu_e}\right)t\right]^{1/2} \quad . \qquad (20)$$

Thus, the island growth at times between the exponential (linear) growth phase and saturated states can be characterized [if $W(0)$ is small] by a scaling that is proportional to t (neoclassical MHD absent) or to $t^{1/2}$ (neoclassical MHD dominant).

Alternately, Eq. (16) can be integrated numerically in time, as shown in Fig. 1a for $\lambda = 2$, $q(0) = 1.34$ [$W(0) = 0.04$] and in Fig. 1b for $\lambda = 1$, $q(0) = 1.34$ [$W(0) = 0.025$] over a range of μ_e/ν_e values. As expected, the saturated island width steadily increases with increasing μ_e/ν_e. The slopes for the t and $t^{1/2}$ scalings are indicated here as a guide. These are not followed for any sizable interval of time because (a) at early times the effect of $W(0)$ can be significant, (b) the drive for island growth is usually a mixture of neoclassical and Δ' effects, and (c) at later times $W(t)$ is no longer $\ll W_{sat}$. These figures are based on the same parameters [i.e., $W(0)$, β_p, r_0, $q(0)$, ϵ] and are plotted on the same scales as the following 3-D numerical results to provide a basis for comparison with the analysis.

Figure 2 shows results from the numerical solution of Eqs. (11)–(13). Here we have removed a section of the early time evolution because it tends to be noisy and have shifted the various runs in time so that they all start at the same island width at a fixed time. Figure 2(a) is for an equilibrium with a q profile of $\lambda = 2$, $q(0) = 1.34$, and Fig. 2(b) is for $\lambda = 1$, $q(0) = 1.34$; these are based on the first density evolution model, which includes only convection (i.e., $\chi_{\|\rho} = 0$). The time evolution characteristics for times intermediate between the early and saturated regimes suggest a weaker growth for the neoclassical cases, closer to the $t^{1/2}$ scaling. The saturated island width increases with μ_e/ν_e up to a certain point and then

tends to become independent of μ_e/ν_e. Following the evolution further in time for the higher values of μ_e/ν_e (> 0.5) indicates that a steady state is not generally achieved and that the island width begins decreasing in time. Such behavior is caused by quasilinear modifications of the q profile, resulting in an inward movement of the resonant surface; this leads to a decreasing island width due to variations in the μ_e/ν_e profile factor and Δ' near the center. However, such longer time scale behaviors are beyond the realm of the present model and are not considered further here.

In some cases in Fig. 2, the island width evolution with neoclassical MHD is somewhat uneven and nonmonotonic. This feature is caused by the strong coupling to the convective density evolution through the fluctuating bootstrap current term. The convective transport moves density into and out of the resonant surface on a time scale that is separate from that of the island evolution. The interaction between these processes can interfere with smooth island evolution.

The $\lambda = 1$ neoclassical MHD results presented in Fig. 2(b) show a proportionately larger departure from the $\mu_e/\nu_e = 0$ limit than the $\lambda = 2$ cases of Fig. 2(a). The cause for this can be seen from Eq. (17), in which Δ'_0 and W_{sat} appear in the denominator of the neoclassical term; as they become smaller (as is the case in going from $\lambda = 2$ to $\lambda = 1$), neoclassical MHD has a relatively greater impact.

The second density evolution model considered here has both convection and parallel diffusion and is expected to yield results closer to those of the analytical model,[8,9] in which a perfectly flat density profile was assumed in the island region. For the values of $\chi_{\|\rho}$ used in these calculations ($\chi_{\|\rho} = 0.5\tau_{Hp}$), the density in the island region is relatively flat and the 2/1 helical projection of constant density contours tends to follow that of the flux contours. Helical flux and density contours (with $\chi_{\|\rho} = 0$ and with $\chi_{\|\rho} = 0.5\tau_{Hp}$) are illustrated in Figs. 3(a) through 3(c). As can be seen, the density contours with $\chi_{\|\rho} = 0.5\tau_{Hp}$ [Fig. 3(c)] have an island structure closer to that of the helical flux contours [Fig. 3(a)] than to those with $\chi_{\|\rho} = 0$ [Fig. 3(b)], which exhibit convective cell regions, as would be expected.

The convective and parallel diffusion density model gives an island time evolution as shown in Fig. 4 for $\lambda = 2$ and $q(0) = 1.34$. The time evolution is generally smoother than for the convection-only cases of Figs. 2(a) and 2(b) because the density equilibrates on a more rapid time scale than the island evolution. These results again show a trend toward the slower $t^{1/2}$ scaling for the larger values of μ_e/ν_e at intermediate times ($70 < t/\tau_{Hp} < 500$) between the exponential growth phase and the saturated nonlinear regime. The saturated island width continues to increase

with μ_e/ν_e up to $\mu_e/\nu_e = 1$, in contrast to the results of Figs. 2(a) and 2(b). Apparently, the bootstrap current is not causing any significant quasilinear modifications to the q profile, as was the case in the convection-only results of Figs. 2(a) and 2(b); also, the density profile in the island region is relatively stationary because of the high level of parallel diffusion.

Figure 5 compares the prediction of Eq. (17) for the dependence of saturated island width on μ_e/ν_e with the results of Figs. 2(a) and 4 for $\lambda = 2$. To avoid ambiguity, we have simply used the maximum island width achieved in the numerical calculations. As mentioned earlier, a true steady state is not always present for the higher values of μ_e/ν_e in Fig. 2(a). The results of the density evolution model with parallel diffusion and convection are closer to the analytical prediction than those obtained with density convection alone. This would be expected because the resulting evolved density profile is closer to that assumed in the analysis underlying Eq. (17). Both models indicate a leveling off in island width at the higher values of μ_e/ν_e. Such deviations at large island widths are due to nonlocal effects and the presence of a conducting wall in the numerical calculations. These effects are not taken into account in the analysis (which is valid for island widths that are small relative to the radius of the resonant $q = m/n$ surface, which $\simeq 0.6$ for the parameters of Fig. 5), so it is not surprising that the analytical and numerical calculations begin to diverge here.

One further parameter dependence of interest for neoclassical tearing instabilities is that with respect to Δ_0', the discontinuity in $\partial\psi/\partial r$ at the resonant surface in the limit of zero island width [defined in association with Eq. (16)]. The perturbed energy δW of conventional linear tearing modes is proportional to Δ_0', resulting in stability for $\Delta_0' < 0$ and instability for $\Delta_0' > 0$. When neoclassical MHD effects are present, the delineation between stability and instability is not directly dependent on the sign of Δ_0' because of the availability of additional instability drive from the fluctuating bootstrap current. We demonstrate this aspect of neoclassical MHD tearing modes by keeping the same $q(r)$ profile as indicated in Eq. (14) and varying q_0. The dependence of Δ_0' on q_0 is displayed in Fig. 6 for the $q(r)$ profile used here with $\lambda = 1.5$. The point where Δ_0' changes sign occurs at $q(0) \simeq 0.9$. This is further verified in Fig. 7, where the island width evolution is followed for $\mu_e/\nu_e = 0$ and $\lambda = 1.5$, starting with an initial 2/1 island width of 0.01. Here the cases for $q(0) = 1.1$ and 1 clearly indicate increasing island size with time. When $q(0) = 0.95$, the island width appears to be decreasing with time, but this is because the saturated island width here is still nonzero but somewhat less than the initial

value of 0.01. The $q(0) = 0.8$ and 0.9 cases are stable and eventually drop to zero island width.

In contrast, Fig. 8 shows the influence of a moderate level of neoclassical MHD ($\mu_e/\nu_e = 0.6$) for $\lambda = 1.5$ and some of the same values of $q(0)$ as in Fig. 7. For all $q(0)$ values here, the tearing instability is linearly unstable and displays monotonic island width growth with time toward a saturated state. This includes values of $q(0)$ for which $\Delta'_0 < 0$ [i.e., $q(0) = 0.8$ and 0.9], which led to decaying island widths in Fig. 7 when neoclassical MHD effects were absent.

IV. CONCLUSIONS

The nonlinear dynamics of single-helicity neoclassical MHD tearing instabilities have been examined by using a 3-D time evolution code in cylindrical geometry. Significant alterations of the usual tearing mode growth are observed, especially at the higher values of neoclassical electron viscosity (μ_e/ν_e). Neoclassical tearing instabilities have increased saturated island widths, which are not solely determined by Δ', and modified growth regimes prior to the nonlinear saturated phase. The threshold for tearing instability is no longer related to the sign of Δ'; unstable cases with finite saturated island widths have been presented here for negative Δ'. In the range of μ_e/ν_e values where island widths are not a sizable fraction of the resonant $q = m/n$ radius, the numerical results compare well with analytic calculations.[8,9] The agreement is particularly good when parallel diffusive losses are included in the density evolution equation, resulting in a flattening of the density profile in the island region similar to that assumed in the analytic model. As μ_e/ν_e is increased to a point where the island width becomes a sizable fraction of the resonant radius, the numerical results begin to depart from the analytic calculation, as might be expected. The numerical island widths are smaller than would be obtained by applying the analysis in this regime. They are, however, still substantially larger than those for the $\mu_e/\nu_e = 0$ case.

The numerical calculations described here provide a number of new features, which extend previous analytic models: (a) the capability to examine various models for density evolution, (b) proper inclusion of the nonlinear coupling to other poloidal modes, and (c) the capability to examine parameter regimes where neoclassical MHD dominates tearing mode growth and island widths can become a sizable fraction of the minor radius. Such calculations will be an important factor

in understanding disruption physics and plasma confinement properties of high-temperature tokamaks operating in long-mean-free-path regimes.

REFERENCES

[1]P. H. Rutherford, *Phys. Fluids* **16**, 1903 (1971).

[2]R. B. White, D. A. Monticello, M. N. Rosenbluth, and B. V. Waddell, *Phys. Fluids* **20**, 800 (1977).

[3]J. D. Callen, B. V. Waddell, B. A. Carreras, M. Azumi, P. J. Catto, H. R. Hicks, J. A. Holmes, D. K. Lee, S. J. Lynch, J. Smith, M. Soler, K. T. Tsang, and J. C. Whitson, in *Proceedings of the 11th International Conference on Plasma Physics and Controlled Nuclear Fusion Research (Kyoto, Japan, November 13–20, 1986)* (International Atomic Energy Agency, Vienna, 1987), Vol. 1, p. 157.

[4]B. V. Waddell, B. A. Carreras, H. R. Hicks, J. A. Holmes, and D. K. Lee, *Phys. Rev. Lett.* **41**, 1386 (1978).

[5]J. D. Callen and K. C. Shaing, see National Technical Service Document No. DE-86009463/XAB (University of Wisconsin Technical Report UWPR 85-8). Copies may be obtained from the National Technical Information Service, Springfield, Virginia 22161. The price is $11.95 plus a $3.00 handling fee. All orders must be prepaid.

[6]J. D. Callen, W. X. Qu, K. D. Siebert, B. A. Carreras, K. C. Shaing, and D. A. Spong, in *Proceedings of the 11th International Conference on Plasma Physics and Controlled Nuclear Fusion Research (Kyoto, Japan, November 13–20, 1986)* (International Atomic Energy Agency, Vienna, 1987), Vol. 2, p. 157.

[7]M. Kotschenreuther, A. Aydemir, R. Carrera, R. D. Hazeltine, J. D. Meiss, and P. J. Morrison, in *Proceedings of the 11th International Conference on Plasma Physics and Controlled Nuclear Fusion Research (Kyoto, Japan, November 13–20, 1986)* (International Atomic Energy Agency, Vienna, 1987), Vol. 2, p. 149.

[8]R. Carrera, R. D. Hazeltine, and M. Kotschenreuther, *Phys. Fluids* **29**, 899 (1986).

[9]W. X. Qu and J. D. Callen, see National Technical Service Document No. DE-86008946/XAB (University of Wisconsin Technical Report UWPR 85-5). Copies may be obtained from the National Technical Information Service, Springfield, Virginia 22161. The price is $11.95 plus a $3.00 handling fee. All orders must be prepaid.

[10]L. Garcia, H. R. Hicks, B. A. Carreras, L. A. Charlton, and J. A. Holmes, see National Technical Service Document No. DE-85018082/XAB (Oak Ridge National Laboratory Technical Report ORNL/TM-9499). Copies may be obtained from the National Technical Information Service, Springfield, Virginia 22161. The price is $11.95 plus a $3.00 handling fee. All orders must be prepaid.

[11]D. A. Spong, K. C. Shaing, B. A. Carreras, J. D. Callen, and L. Garcia, "Transition from Resistive Ballooning to Neoclassical Magnetohydrodynamic Pressure-Gradient-Driven Instability," to be submitted to *The Physics of Fluids*.

FIGURE CAPTIONS

Fig. 1. Time evolution of island width for a range of values of μ_e/ν_e for (a) $\lambda = 2$, $q(0) = 1.34$, and (b) $\lambda = 1$, $q(0) = 1.34$.

Fig. 2. Time evolution of island width from the 3-D numerical calculations in cylindrical geometry for a range of values of μ_e/ν_e with only density convection for (a) $\lambda = 2$, $q(0) = 1.34$ and (b) $\lambda = 1$, $q(0) = 1.34$.

Fig. 3. 2/1 helical projections: (a) typical flux contours, (b) density contours with convection only ($\chi_{\|\rho} = 0$), and (c) density contours with convection and parallel diffusion ($\chi_{\|\rho} = 0.5\ \tau_{Hp}$).

Fig. 4. Time evolution of island width from the 3-D numerical calculations in cylindrical geometry for $\lambda = 2$, $q(0) = 1.34$ for a range of values of μ_e/ν_e with density convection and parallel diffusion.

Fig. 5. Comparison of island width dependence on μ_e/ν_e between analytical theory (solid line) and the two density evolution models.

Fig. 6. Dependence of Δ_0' on central q value, $q(0)$.

Fig. 7. Dependence of tearing mode island width evolution on central q value for $\lambda = 1.5$, $\mu_e/\nu_e = 0$ (neoclassical MHD absent).

Fig. 8. Dependence of tearing mode island width evolution on central q value for $\lambda = 1.5$ with neoclassical MHD ($\mu_e/\nu_e = 0.6$).

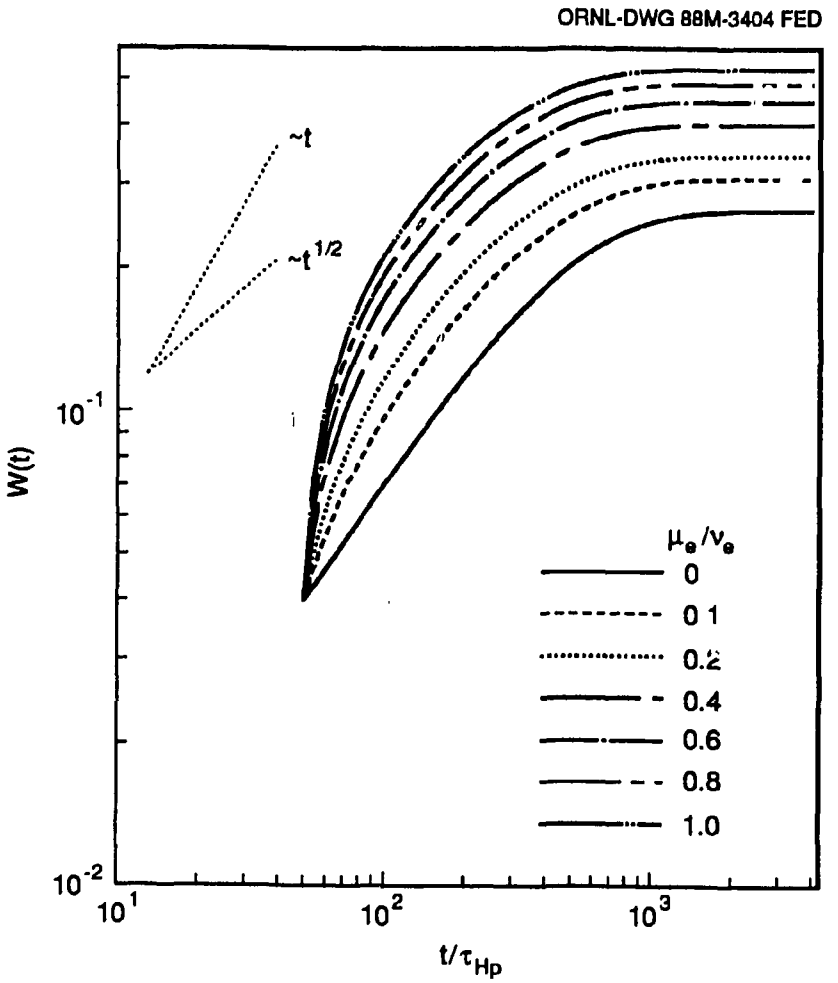
ORNL-DWG 88M-3404 FED
~t
~t^1/2
W(t)
10^-1
10^-2
10^1
10^2
10^3
t/τ_Hp
μ_e/ν_e
0
0.1
0.2
0.4
0.6
0.8
1.0

Fig. 1(a)

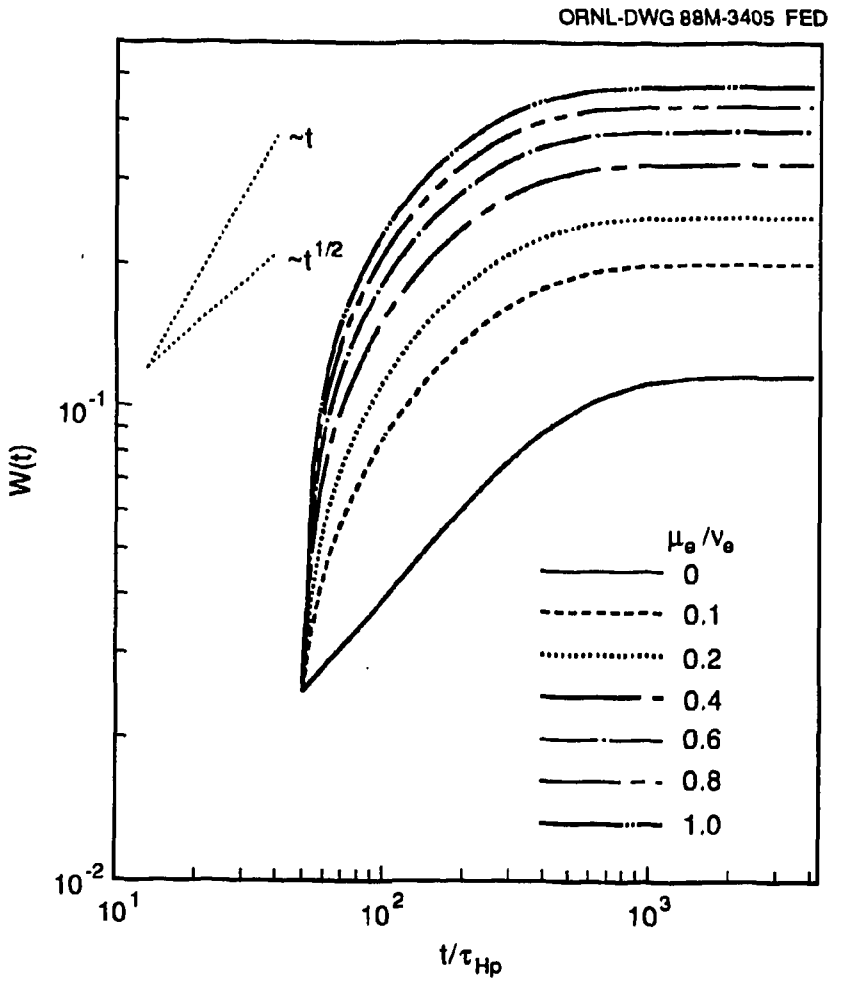
ORNL-DWG 88M-3405 FED
~t
~t^1/2
10^-1
10^-2
W(t)
10^1
10^2
10^3
t/τ_Hp
μ_e /ν_e
0
0.1
0.2
0.4
0.6
0.8
1.0

Fig. 1(b)

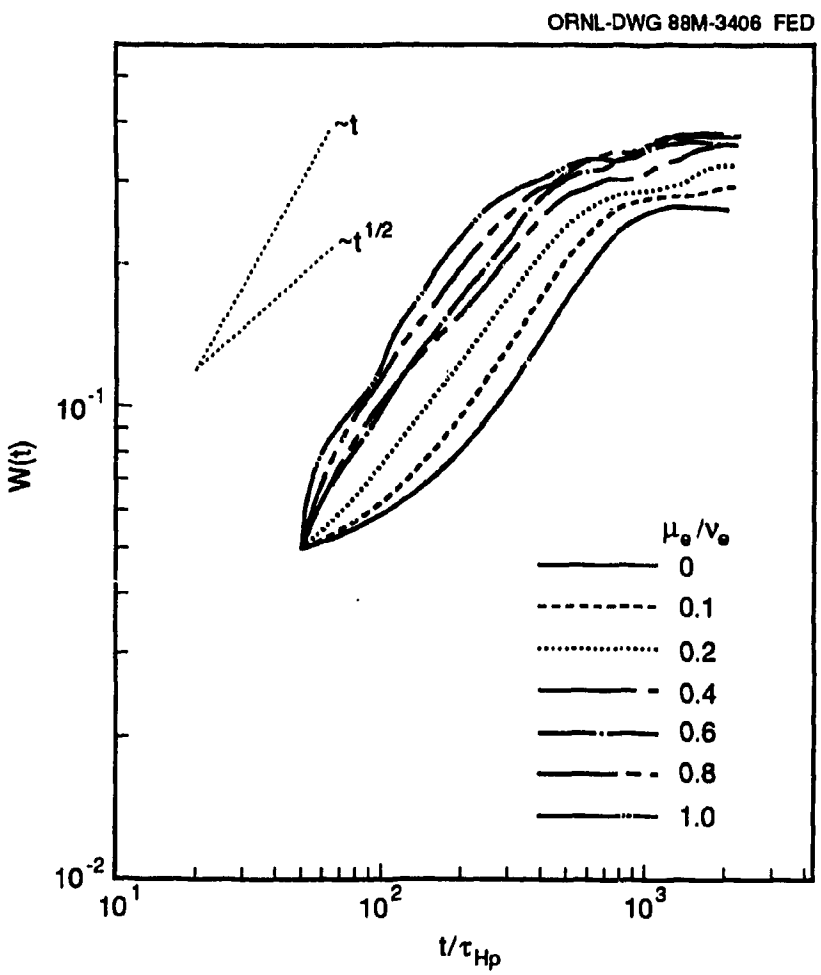
ORNL-DWG 88M-3406 FED
~t
~t^1/2
W(t)
10^-1
10^-2
10^1
10^2
10^3
t/τ_Hp
μ_e/ν_e
0
0.1
0.2
0.4
0.6
0.8
1.0

Fig. 2(a)

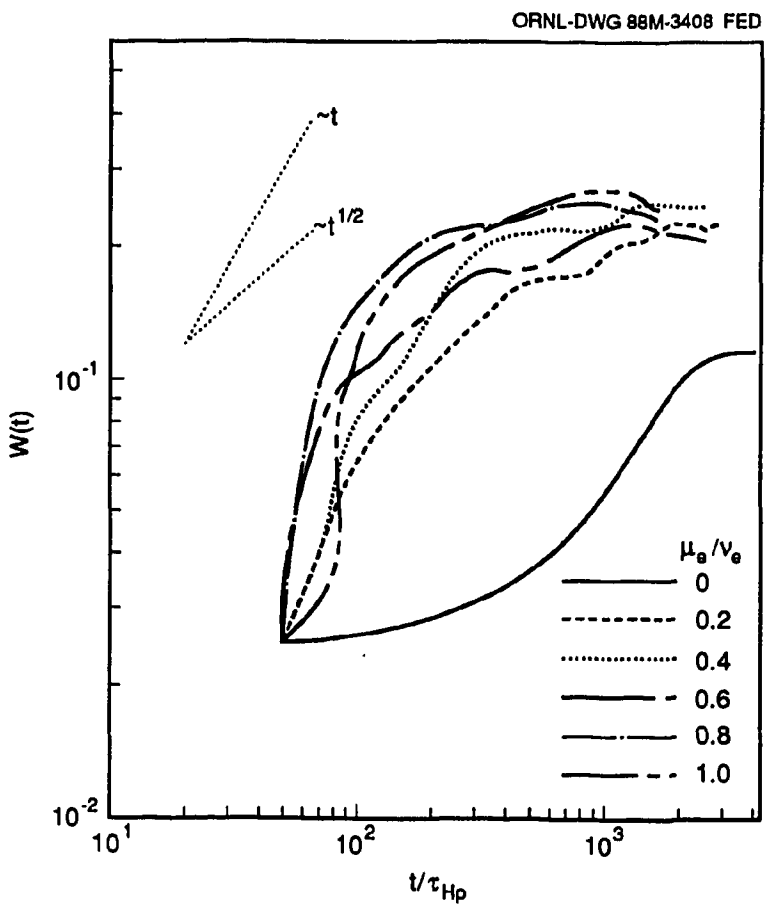
ORNL-DWG 88M-3408 FED
~t
~t^1/2
W(t)
10^-1
10^-2
10^1
10^2
10^3
t/τ_Hp
μ_e/ν_e
0
0.2
0.4
0.6
0.8
1.0

Fig. 2(b)

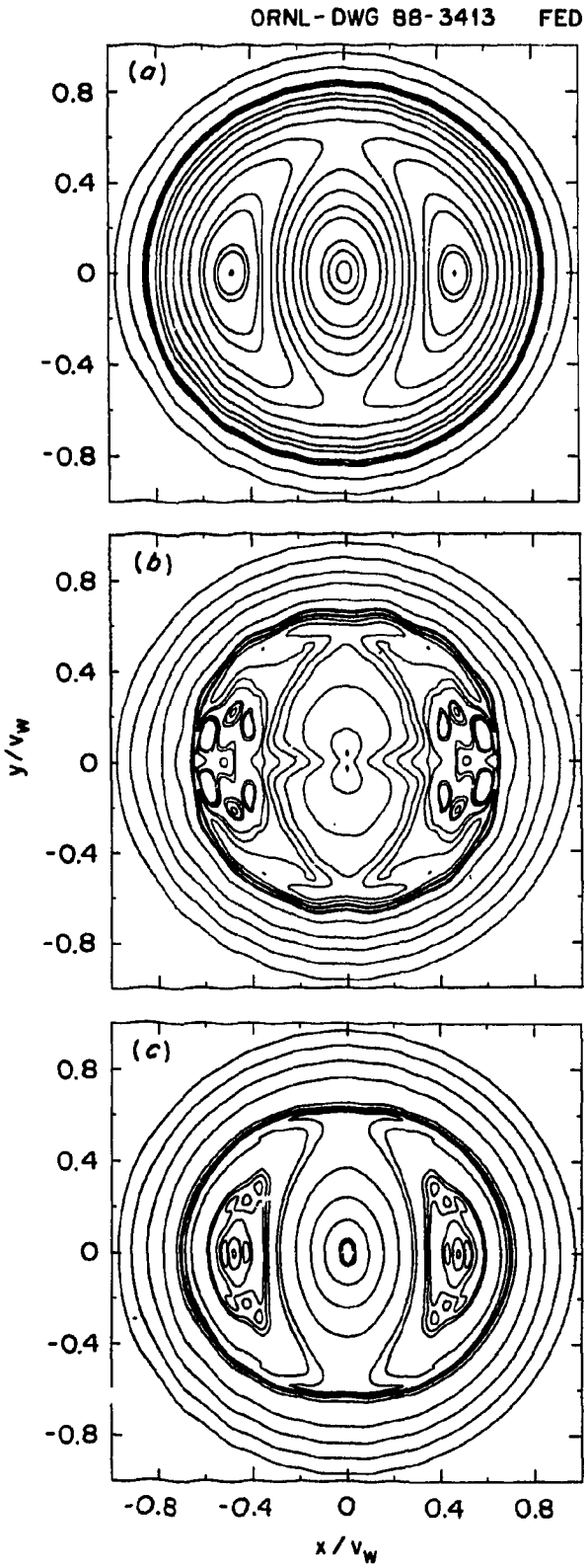

Fig. 3

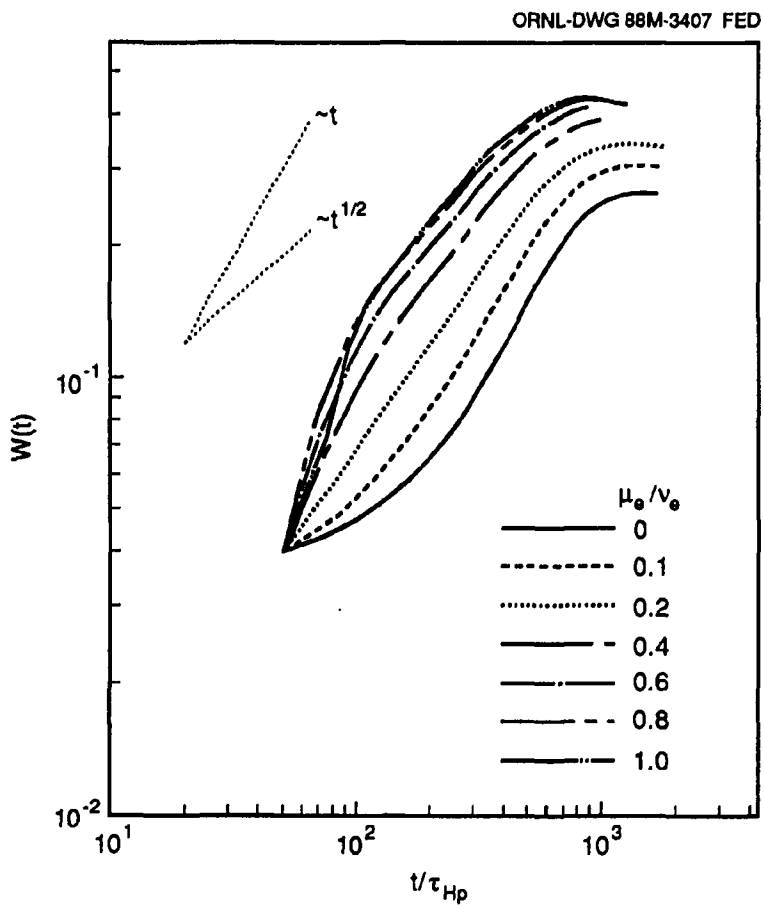
ORNL-DWG 88M-3407 FED
~t
~t^1/2
W(t)
10^-1
10^-2
10^1
10^2
10^3
t/τ_Hp
μ_e/ν_e
0
0.1
0.2
0.4
0.6
0.8
1.0

Fig. 4

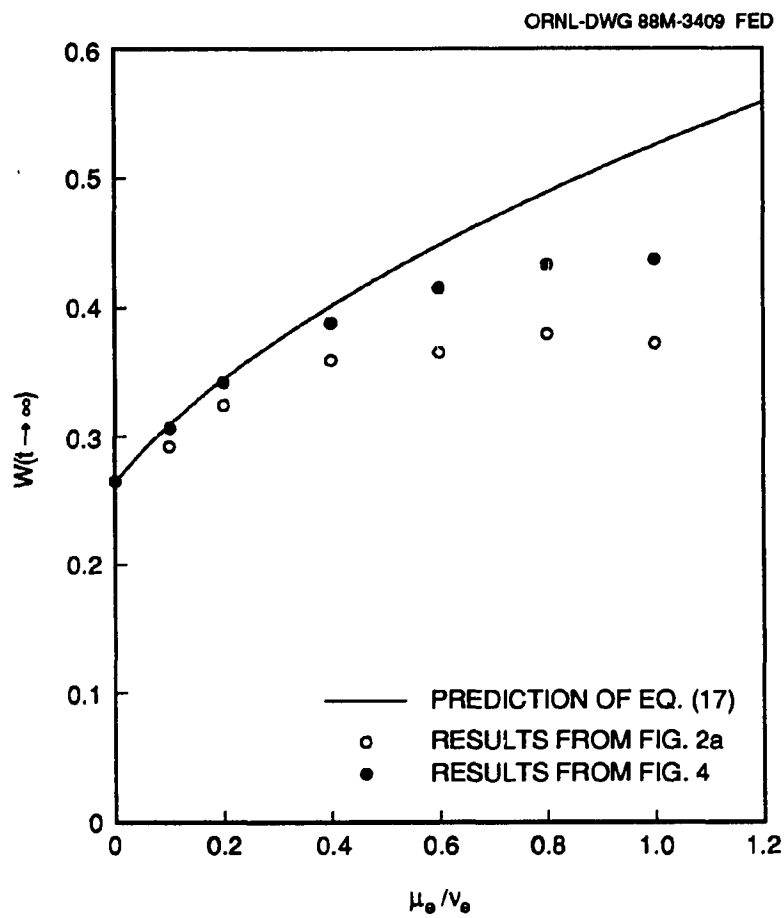
ORNL-DWG 88M-3409 FED
0.6
0.5
0.4
0.3
0.2
0.1
0
W(t → ∞)
0
0.2
0.4
0.6
0.8
1.0
1.2
μe/νe
PREDICTION OF EQ. (17)
RESULTS FROM FIG. 2a
RESULTS FROM FIG. 4

Fig. 5

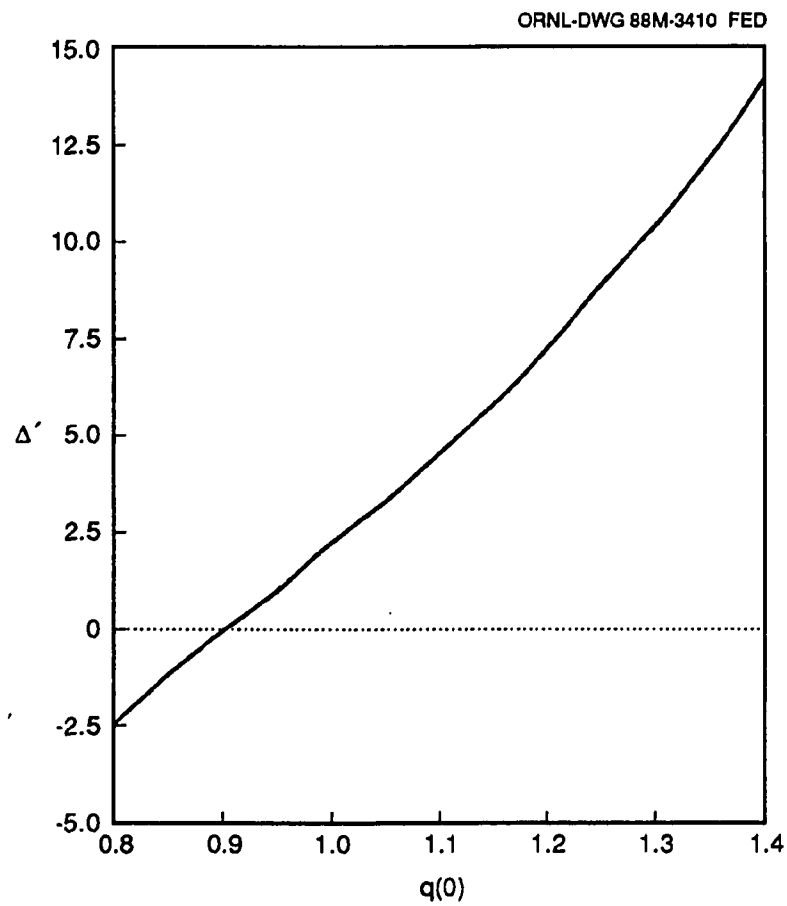
ORNL-DWG 88M-3410 FED
15.0
12.5
10.0
7.5
Δ′ 5.0
2.5
0
-2.5
-5.0
0.8
0.9
1.0
1.1
1.2
1.3
1.4
q(0)

Fig. 6

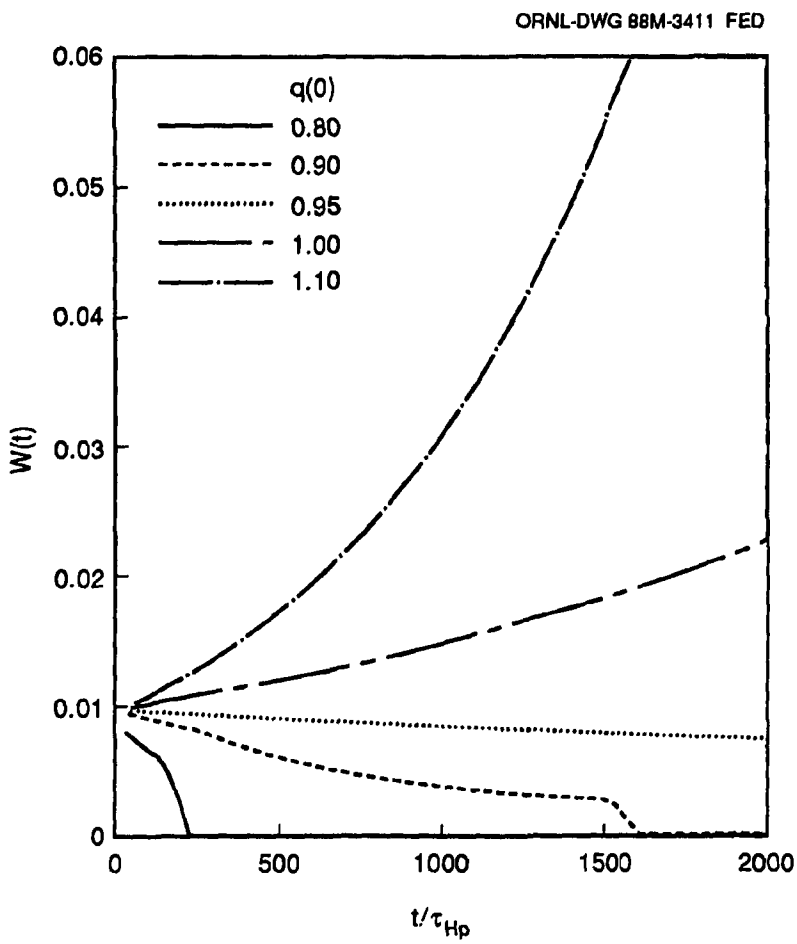
ORNL-DWG 88M-3411 FED
q(0)
0.80
0.90
0.95
1.00
1.10
W(t)
0.06
0.05
0.04
0.03
0.02
0.01
0
0
500
1000
1500
2000
t/τHp

Fig. 7

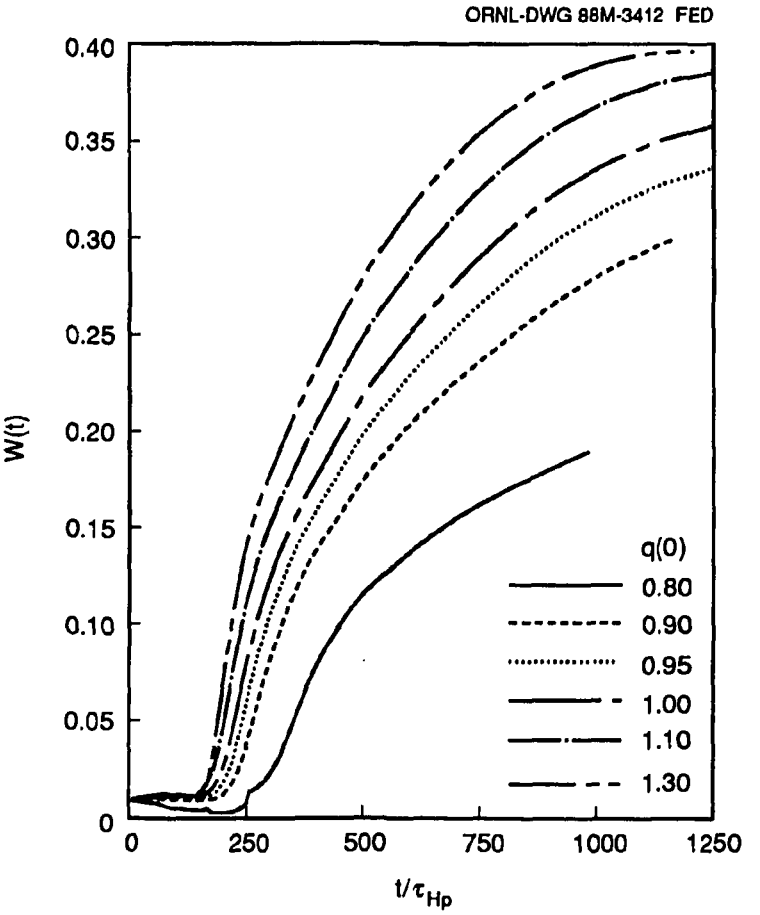
ORNL-DWG 88M-3412 FED
0.40
0.35
0.30
0.25
0.20
0.15
0.10
0.05
0
W(t)
0
250
500
750
1000
1250
t/τHp
q(0)
0.80
0.90
0.95
1.00
1.10
1.30

Fig. 8

ORNL/TM-10947
Dist. Category UC-427

INTERNAL DISTRIBUTION

1. L. A. Berry
2–3. B. A. Carreras
4–5. L. A. Charlton
6. N. Dominguez
7. R. A. Dory
8. C. L. Hedrick
9. S. P. Hirshman
10. J. A. Holmes
11. W. A. Houlberg
12. G. S. Lee
13. J-N. LeBeouf
14. V. E. Lynch
15–16. K. C. Shaing
17. J. Sheffield
18–22. D. A. Spong
23–24. Laboratory Records Department
25. Laboratory Records, ORNL-RC
26. Central Research Library
27. Document Reference Section
28. Fusion Energy Division Library
29–30. Fusion Energy Division Publications Office
31. ORNL Patent Office

EXTERNAL DISTRIBUTION

32. Office of the Assistant Manager for Energy Research and Development, U.S. Department of Energy, Oak Ridge Operations Office, P.O. Box E, Oak Ridge, TN 37831
33–34. J. D. Callen, Department of Nuclear Engineering, University of Wisconsin, Madison, WI 53706-1687
35. J. F. Clarke, Director, Office of Fusion Energy, Office of Energy Research, ER-50 Germantown, U.S. Department of Energy, Washington, DC 20545
36. R. W. Conn, Department of Chemical, Nuclear, and Thermal Engineering, University of California, Los Angeles, CA 90024
37. S. O. Dean, Fusion Power Associates, Inc., 2 Professional Drive, Suite 248, Gaithersburg, MD 20879
38. H. K. Forsen, Bechtel Group, Inc., Research Engineering, P. O. Box 3965, San Francisco, CA 94119
39. J. R. Gilleland, L-644, Lawrence Livermore National Laboratory, P.O. Box 5511, Livermore, CA 94550
40. R. W. Gould, Department of Applied Physics, California Institute of Technology, Pasadena, CA 91125
41. R. A. Gross, Plasma Research Laboratory, Columbia University, New York, NY 10027
42. D. M. Meade, Princeton Plasma Physics Laboratory, P.O. Box 451, Princeton, NJ 08543

43. M. Roberts, International Programs, Office of Fusion Energy, Office of Energy Research, ER-52 Germantown, U.S. Department of Energy, Washington, DC 20545
44. W. M. Stacey, School of Nuclear Engineering and Health Physics, Georgia Institute of Technology, Atlanta, GA 30332
45. D. Steiner, Nuclear Engineering Department, NES Building, Tibbetts Avenue, Rensselaer Polytechnic Institute, Troy, NY 12181
46. R. Varma, Physical Research Laboratory, Navrangpura, Ahmedabad 380009, India
47. Bibliothek, Max-Planck Institut für Plasmaphysik, Boltzmannstrasse 2, D-8046 Garching, Federal Republic of Germany
48. Bibliothek, Institut für Plasmaphysik, KFA Jülich GmbH, Postfach 1913, D-5170 Jülich, Federal Republic of Germany
49. Bibliothek, KfK Karlsruhe GmbH, Postfach 3640, D-7500 Karlsruhe 1, Federal Republic of Germany
50. Bibliotheque, Centre de Recherches en Physique des Plasmas, Ecole Polytechnique Fédérale de Lausanne, 21 Avenue des Bains, CH-1007 Lausanne, Switzerland
51. R. Aymar, CEN/Cadarache, Departement de Recherches sur la Fusion Contrôlée, F-13108 Saint-Paul-lez-Durance Cedex, France
52. Bibliothèque, CEN/Cadarache, F-13108 Saint-Paul-lez-Durance Cedex, France
53. Library, Culham Laboratory, UKAEA, Abingdon, Oxfordshire, OX14 3DB, England
54. Library, JET Joint Undertaking, Abingdon, Oxfordshire OX14 3EA, England
55. Library, FOM-Instituut voor Plasmafysica, Rijnhuizen, Edisonbaan 14, 3439 MN Nieuwegein, The Netherlands
56. Library, Institute of Plasma Physics, Nagoya University, Chikusa-ku, Nagoya 464, Japan
57. Library, International Centre for Theoretical Physics, P.O. Box 586, I-34100 Trieste, Italy
58. Library, Centro Richerche Energia Frascati, C.P. 65, I-00044 Frascati (Roma), Italy
59. Library, Plasma Physics Laboratory, Kyoto University, Gokasho, Uji, Kyoto 611, Japan
60. Plasma Research Laboratory, Australian National University, P.O. Box 4, Canberra, A.C.T. 2601, Australia
61. Library, Japan Atomic Energy Research Institute, Naka Fusion Research Establishment, 801-1 Mukoyama, Naka-machi, Naka-gun, Ibaraki-ken, Japan
62. G. A. Eliseev, I. V. Kurchatov Institute of Atomic Energy, P. O. Box 3402, 123182 Moscow, U.S.S.R.

63. V. A. Glukhikh, Scientific-Research Institute of Electro-Physical Apparatus, 188631 Leningrad, U.S.S.R.
64. I. Shpigel, Institute of General Physics, U.S.S.R. Academy of Sciences, Ulitsa Vavilova 38, Moscow, U.S.S.R.
65. D. D. Ryutov, Institute of Nuclear Physics, Siberian Branch of the Academy of Sciences of the U.S.S.R., Sovetskaya St. 5, 630090 Novosibirsk, U.S.S.R.
66. V. T. Tolok, Kharkov Physical-Technical Institute, Academical St. 1, 310108 Kharkov, U.S.S.R.
67. Deputy Director, Southwestern Institute of Physics, P.O. Box 15, Leshan, Sichuan, China (PRC)
68. Director, The Institute of Plasma Physics, P.O. Box 26, Hefei, Anhui, China (PRC)
69. D. Crandall, Experimental Plasma Research Branch, Division of Development and Technology, Office of Fusion Energy, Office of Energy Research, ER-542 Germantown, U.S. Department of Energy, Washington, DC 20545
70. N. A. Davies, Office of the Associate Director, Office of Fusion Energy, Office of Energy Research, ER-51 Germantown, U.S. Department of Energy, Washington, DC 20545
71. R. H. McKnight, Experimental Plasma Research Branch, Division of Development and Technology, Office of Fusion Energy, Office of Energy Research, ER-542 Germantown, U.S. Department of Energy, Washington, DC 20545
72. D. B. Nelson, Director, Division of Applied Plasma Physics, Office of Fusion Energy, Office of Energy Research, ER-54 Germantown, U.S. Department of Energy, Washington, DC 20545
73. E. Oktay, Division of Confinement Systems, Office of Fusion Energy, Office of Energy Research, ER-55 Germantown, U.S. Department of Energy, Washington, DC 20545
74. W. Sadowski, Fusion Theory and Computer Services Branch, Division of Applied Plasma Physics, Office of Fusion Energy, Office of Energy Research, ER-541 Germantown, U.S. Department of Energy, Washington, DC 20545
75. R. E. Mickens, Atlanta University, Department of Physics, Atlanta, GA 30314
76. M. N. Rosenbluth, University of California–San Diego, La Jolla, CA 92093-0319
77. Duk-In Choi, Department of Physics, Korea Advanced Institute of Science and Technology, P.O. Box 150, Chong Ryang-Ri, Seoul, Korea
78. Library of Physics Department, University of Ioannina, Ioannina, Greece
79. C. De Palo, Library, Associazione EURATOM-ENEA sulla Fusione, CP 65, I-00044 Frascati (Roma), Italy
80. Theory Department Read File, c/o D. W. Ross, University of Texas, Institute for Fusion Studies, Austin, TX 78712

81. Theory Department Read File, c/o R. Parker, Director, Plasma Fusion Center, NW 16-202, Massachusetts Institute of Technology, Cambridge, MA 02139
82. Theory Department Read File, c/o R. White, Princeton Plasma Physics Laboratory, P.O. Box 451, Princeton, NJ 08543
83. Theory Department Read File, c/o L. Kovrizhnykh, Lebedev Institute of Physics, Academy of Sciences, 53 Leninsky Prospect, 117924 Moscow, U.S.S.R.
84. Theory Department Read File, c/o B. B. Kadomtsev, I. V. Kurchatov Institute of Atomic Energy, P.O. Box 3402, 123182 Moscow, U.S.S.R.
85. Theory Department Read File, c/o T. Kamimura, Institute of Plasma Physics, Nagoya University, Nagoya 464, Japan
86. Theory Department Read File, c/o C. Mercier, Departemente de Recherches sur la Fusion Controlee, B.P. No. 6, F-92260 Fontenay-aux-Roses (Seine), France
87. Theory Department Read File, c/o T. E. Stringer, JET Joint Undertaking, Abingdon, Oxfordshire OX14 3EA, United Kingdom
88. Theory Department Read File, c/o R. Briscoe, Culham Laboratory, Abingdon, Oxfordshire OX14 3DB, United Kingdom
89. Theory Department Read File, c/o D. Biskamp, Max-Planck-Institut für Plasmaphysik, Boltzmannstrasse 2, D-8046 Garching, Federal Republic of Germany
90. Theory Department Read File, c/o T. Takeda, Japan Atomic Energy Research Institute, Tokai Fusion Research Establishment, Tokai-mura, Nakagun, Ibaraki-ken, Japan
91. Theory Department Read File, c/o J. Greene, General Atomics, P.O. Box 85608, San Diego, CA 92138
92. Theory Department Read File, c/o L. D. Pearlstein, L-630, Lawrence Livermore National Laboratory, P.O. Box 5511, Livermore, CA 94550
93. Theory Department Read File, c/o R. Gerwin, CTR Division, Los Alamos National Laboratory, P.O. Box 1663, Los Alamos, NM 87545

94–95. L. Garcia, Universidad Complutense, Madrid, Spain

96. H. Biglari, University of California–San Diego, La Jolla, CA 92093-0319
97. R. Bonomo, ECE Department, University of Wisconsin, 1415 Johnson Dr., Madison, WI 53706
98. C. P. T. Bussac, École Polytechnique, F-91120 Palaiseau, France
99. Z. Chang, Physics Department, University of Wisconsin, Madison, WI 53706
100. L. Chen, Princeton Plasma Physics Laboratory, P.O. Box 451, Princeton, NJ 08543
101. C. Z. Cheng, Princeton Plasma Physics Laboratory, P.O. Box 451, Princeton, NJ 08543
102. S. T. Chun, Courant Institute of Mathematical Sciences, New York University, 251 Mercer St., New York, NY 10012

103. J. W. Connor, Culham Laboratory, UKAEA, Abingdon, Oxon OX14 3DB, England
104. P. H. Diamond, University of California–San Diego, La Jolla, CA 92093-0319
105. K. Dimoff, INRS-Energie, C.P. 1020, Varennes, Quebec JOL 2PO, Canada
106. A. H. Glasser, CTR-6 Group, MS-F642, Los Alamos National Laboratory, P.O. Box 1663, Los Alamos, NM 87545
107. J. Greene, General Atomics, P.O. Box 85608, San Diego, CA 92138-5608
108. B. Guss, NW17-172, MIT Plasma Fusion Center, 175 Albany St., Cambridge, MA 02139
109. T. S. Hahm, Princeton Plasma Physics Laboratory, P.O. Box 451, Princeton, NJ 08543
110. R. J. Hastie, Culham Laboratory, UKAEA, Abingdon, Oxon OX14 3DB, England
111. T. C. Hender, Culham Laboratory, UKAEA, Abingdon, Oxon OX14 3DB, England
112. J. Johnson, Princeton Plasma Physics Laboratory, P.O. Box 451, Princeton, NJ 08543
113. S. K. Kim, Fusion Research Center, University of Texas, Austin, TX 78712
114. Y. B. Kim, University of California–San Diego, La Jolla, CA 92093-0319
115. Y. B. Kim, University of Wisconsin, Madison, WI 53706
116. M. Kotschenreuther, Institute for Fusion Studies, University of Texas, Austin, TX 78712
117. O. J. Kwon, University of California–San Diego, La Jolla, CA 92093-0319
118. C. S. Liu, Department of Physics and Astronomy, University of Maryland, College Park, MD 20742
119. S. Migliuolo, 26-205, Massachusetts Institute of Technology, Cambridge, MA 02139
120. F. Perkins, Princeton Plasma Physics Laboratory, P.O. Box 451, Princeton, NJ 08543
121. G. Rewoldt, Princeton Plasma Physics Laboratory, P.O. Box 451, Princeton, NJ 08543
122. K. S. Riedel, New York University 251 Mercer St., New York, NY 10012
123. D. J. Sigmar, NW16-243, MIT Plasma Fusion Center, 167 Albany St., Cambridge, MA 02139
124. A. Sykes, Culham Laboratory, UKAEA, Abingdon, Oxon OX14 3DB, England
125. J. Weiland, Institute for Electromagnetic Field Theory and EURATOM–Fusion Research (SERC), Chalmers University of Technology, S-412 96 Göteborg, Sweden

126–171. Given distribution according to DOE/OSTI-4500, Energy Research (Distribution Category UC-427, Theoretical Plasma Physics)